

HIERARCHICAL ORTHOGONAL FACTORIZATION: SPARSE LEAST SQUARES PROBLEMS*

ABEYNAYA GNANASEKARAN[†] AND ERIC DARVE[†]

Abstract. In this work, we develop a fast hierarchical solver for solving large, sparse least squares problems. We build upon the algorithm, spaQR (sparsified QR [16]), that was developed by the authors to solve large sparse linear systems. Our algorithm is built on top of a Nested Dissection based multifrontal QR approach. We use low-rank approximations on the frontal matrices to sparsify the vertex separators at every level in the elimination tree. Using a two-step sparsification scheme, we reduce the number of columns and maintain the ratio of rows to columns in each front without introducing any additional fill-in. With this improvised scheme, we show that the runtime of the algorithm scales as $\mathcal{O}(M \log N)$ and uses $\mathcal{O}(M)$ memory to store the factorization. This is achieved at the expense of a small and controllable approximation error. The end result is an approximate factorization of the matrix stored as a sequence of sparse orthogonal and upper-triangular factors and hence easy to apply/solve with a vector. Finally, we compare the performance of the spaQR algorithm in solving sparse least squares problems with direct multifrontal QR and CGLS iterative method with a standard diagonal preconditioner.

1. Introduction. In this work, we are interested in solving large sparse linear least squares problems of the form,

$$(1.1) \quad \min_x \|Ax - b\|_2, \quad A \in \mathbb{R}^{M \times N}, \quad M \geq N, \quad \text{rank}(A) = N$$

Least squares problems appear in a wide range of topics ranging from constrained optimization, computer graphics to economics, data analysis and machine learning. These typically have millions of rows and columns but in many applications may have less than 0.1% of the entries that are non-zero. It is therefore important to maintain the sparsity of the matrix for efficient solutions to large sparse least squares problems.

The most commonly used technique to solve the least squares problems is to solve the normal equations,

$$(1.2) \quad A^T A x = A^T b$$

The solution to the normal equations is also the solution to the least squares problem given in Equation (1.1). The normal equations form a symmetric positive definite linear system which can be solved with a sparse Cholesky factorization or an iterative method like CG [21]. However, the condition number of the coefficient matrix $A^T A$ in the normal equations is square of the condition number of A . Hence, explicitly forming $A^T A$ and solving the normal equations may lead to numerical instabilities. As a result, this method is not appropriate for ill-conditioned or stiff problems [4, 18].

A more reliable and accurate direct method for least squares problems is using the QR decomposition of A . Then, solving Equation (1.1) boils down to the solution of the linear system,

$$R x = Q^T b$$

*Submitted to the editors on February 22, 2021

Funding: This work was partly funded by a grant from Sandia National Laboratories (Laboratory Directed Research and Development [LDRD]) entitled “Hierarchical Low-rank Matrix Factorizations,” and a grant from the National Aeronautics and Space Administration (NASA, agreement #80NSSC18M0152).

[†]Institute for Computational and Mathematical Engineering, Stanford University, CA (abeynaya@stanford.edu), (darve@stanford.edu)

In general, the orthogonal factor Q is not stored to save on the available memory. In this case, the solution can be computed using the corrected seminormal equations (CSNE) approach of [3]. This involves solving,

$$R^T R \bar{x} = A^T b$$

along with one step of iterative refinement. The error analysis in [3] shows that the solution computed this way is of high accuracy. Finally, note that the R factor in the QR decomposition is also the Cholesky factor of $A^T A$. However, the use of orthogonal transformations in the QR decomposition make the factorization stable as opposed to computing the Cholesky decomposition of $A^T A$.

Direct methods can be expensive even for sparse matrices due to the fill-in (new non-zero entries) introduced during the factorization. On the other hand, iterative methods such as CGLS [17], LSQR [33], LSMR [13], which have been proposed for least-squares problems, rarely work well without good preconditioners. A good hybrid between the two are preconditioned iterative methods, where a preconditioner is built based on an approximate factorization of the matrix. For example, Incomplete Cholesky (on $A^T A$) [31], Incomplete QR (IQR) [26, 36], Multilevel Incomplete QR (MIQR) [30] find an approximate factorization by thresholding the fill-in entries. In general, these preconditioners are not guaranteed to work and can fail for a large number of problems [25, 6, 38]. Better preconditioners can be built when additional information on the problem is available.

The spaQR algorithm developed by the authors for solving linear systems in [16] is built on the idea that certain off-diagonal blocks in A and $A^T A$ are low-rank. It is known that matrices arising out of partial differential equations have this property. We exploited this to build a fast approximate sparse QR factorization of A and use it as a preconditioner to solve linear systems in $\mathcal{O}(N \log N)$ time [16]. However for tall, thin matrices (least squares problems), we will not have a near linear algorithm if we use spaQR algorithm as such without any modifications. In this work, we propose modifications to the original spaQR algorithm that can be used to solve linear least squares problems also in near linear time.

SpaQR is an example of a hierarchical solver that works by decreasing the size of the vertex separators in each level of a Nested Dissection partitioning of the matrix. Other examples of hierarchical solvers include the Hierarchical Interpolative Factorization (HIF) [22, 23, 11, 12], LoRaSp [35, 42] and Sparsified Nested Dissection (spaND) [5, 29]. All three solvers were developed to perform a fast Cholesky factorization of SPD matrices by incorporating low-rank approximations in the classical multifrontal approach. Some of these algorithms were later extended to perform a fast LU factorization on unsymmetric matrices [22]. In contrast, another popular approach is to store the dense fronts using low-rank bases and perform fast matrix-vector products using these bases [1, 2, 10, 15, 34, 37, 40, 41]. Most of the efforts in this area have been focused on solving linear systems and has recently been extended to solve Toeplitz least squares problems [39].

The (new) spaQR algorithm produces a sparse orthogonal factorization of $A \in \mathbb{R}^{M \times N}$ in $\mathcal{O}(M \log N)$ time, such that,

$$A \approx QW = \prod_i Q_i \prod_j W_j$$

where each Q_i is a sparse orthogonal matrix and W_j is either a sparse orthogonal or sparse upper triangular matrix. Note that while the W factor is not strictly upper

triangular, we still use the term “fast QR solver” as the algorithm is built on top of the multifrontal QR method. To the best of our knowledge, this is the first work of its kind to combine the ideas of low-rank approximations and QR factorization to build a fast sparse least squares solver.

In the rest of the paper, we discuss the algorithm in detail and provide theoretical and numerical results to validate our claims.

1.1. Contribution. We extend the spaQR algorithm developed in [16] to solve linear least squares problem. Our main contributions are as follows:

- We introduce a way to reorder and sparsify the rows in addition to the columns in the sparse multifrontal QR factorization for tall, thin matrices.
- Under some assumptions, we show that the factorization time scales as $\mathcal{O}(M \log N)$ ■
- We show numerical benchmarks on least squares problems arising in PDE constrained optimization problems and on matrices taken from the Suite Sparse Matrix Collection [7].
- The C++ code for the implementation is freely available for download and use¹. The benchmarks can be reproduced by using the scripts available in the repository.

Organization of the paper. In Section 2, we review the spaQR algorithm for solving linear systems and extend it solve least squares problems. We discuss the complexity of the algorithm in Section 3. Finally, in Section 4, we provide numerical results on benchmark problems.

2. Algorithm. The spaQR algorithm is built on top of a sparse multifrontal QR factorization. The matrix is represented as a collection of dense blocks partitioned using a Nested Dissection based scheme. The key idea in the spaQR algorithm is to continually reduce the number of columns (and an equal number of rows) of the frontal matrices giving a $\mathcal{O}(N \log N)$ algorithm for solving linear systems.

However, for least squares problems, we also need to control the aspect ratio of each diagonal block (i.e., the ratio number of rows / number of columns) in the matrix. For example, if the spaQR algorithm is used as such, we will end up with a final block that has few columns but $O(M)$ rows (i.e., the aspect ratio is unbounded), which would lead to a high computational cost. So controlling the aspect ratio of the diagonal blocks is a key step in our new algorithm.

We begin with a brief review of the spaQR algorithm for solving linear systems (square matrices). Then, we explain the improvements needed to handle least squares problems where the matrix is now tall and thin. In particular, we describe a row reordering strategy and additional sparsification steps.

2.1. Sparsified QR (spaQR) for square matrices. The spaQR algorithm was proposed by the authors in [16] to perform an approximate QR factorization of a sparse square matrix in $\mathcal{O}(N \log N)$ time. The algorithm is built on top of a sparse multifrontal QR factorization. The key step is to continually decrease the size of the vertex separators (obtained using Nested Dissection) by using a low-rank approximation of its off-diagonal blocks. Here, we go over the algorithm and introduce key terminology that will be used in the rest of the paper.

Multifrontal methods are organized as a sequence of factorizations of small dense matrices. The order of factorization is given by the elimination tree and the factorization proceeds from the leaves to the root of the tree. Prior to the factorization, the matrix is typically reordered to minimize the fill-in (new non-zero entries) that

¹https://github.com/Abeynaya/spaQR_public

appear during the factorization. We use a Nested Dissection ordering for this purpose as it typically leads to minimal fill-in [14].

For computational efficiency, we need to block or partition the separators at every level of the tree. This partitioning needs to be done at all levels, not simply at the level at which the separator was computed. For example, Figures 1, 3b, and 3c show the multilevel partitioning of the top separator. The top separator is the dark grey separator in the center.

In the rest of the paper, we will call each block in this partition an interface. Figure 1 shows a 3-level Nested Dissection partition of an arbitrary graph; the figure on the left shows the Nested Dissection separators and the one on the right shows the interfaces. To minimize the number of floating point operations and the rank of the off-diagonal blocks, it is best if an interface is connected to few subdomains in the nested dissection. At a minimum, an interface will be connected to two subdomains. But because of the way separators are constructed, we will also have small interfaces that are connected to three or more subdomains.

The spaQR algorithm alternates between factoring (block QR) the separators at a level l , scaling and sparsifying the ‘interfaces’ at all levels $l' > l$ in the elimination tree.

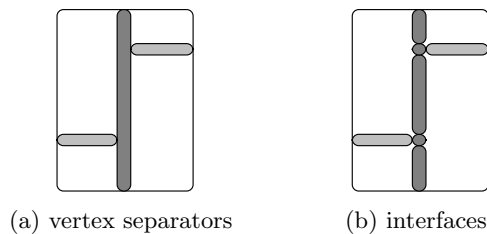


Fig. 1: Nested dissection partition with 3 levels. The figure on the left shows the vertex separators and the one on the right shows the interfaces.

Consider the spaQR algorithm with a simple 3-level Nested Dissection partitioning as shown in Figure 1. The spaQR algorithm first performs a block QR factorization on each interior (white region in Figure 1). Then, it scales and sparsifies the interfaces belonging to the remaining separators as discussed next. Consider a subset of the top separator in Figure 1 that is at the interface between two interiors. Let p be the interface and n be all the nodes in the subdomains connected to the interface. Then, the associated block in the matrix is,

$$A_p = \begin{bmatrix} A_{pp} & A_{pn} \\ A_{np} & A_{nn} \end{bmatrix}$$

Assume that the block $A_{pp} = I$. This is not a limiting assumption, as we perform a block diagonal scaling on the interfaces (see Subsection 2.4) before sparsification. The key assumption in the spaQR algorithm is that the off-diagonal blocks (A_{pn} , A_{np}) are low-rank. Compute a low-rank approximation of,

$$\begin{bmatrix} A_{np}^T & A_{pn} \end{bmatrix} = Q_{pp} W_{pn} = \begin{bmatrix} Q_{pf} & Q_{pc} \end{bmatrix} \begin{bmatrix} W_{fn} \\ W_{cn} \end{bmatrix} \text{ with } \|W_{fn}\|_2 = \mathcal{O}(\epsilon)$$

Then apply Q_{pp} to A ,

$$\begin{bmatrix} Q_{pp} & \\ & I \end{bmatrix}^T \begin{bmatrix} I & A_{pn} \\ A_{np} & A_{nn} \end{bmatrix} \begin{bmatrix} Q_{pp} & \\ & I \end{bmatrix} = \begin{bmatrix} I & & \mathcal{O}(\epsilon) \\ & I & \hat{A}_{cn} \\ \mathcal{O}(\epsilon) & \hat{A}_{nc} & A_{nn} \end{bmatrix}$$

Thus by applying the orthogonal transformation Q , we split the nodes of interface p into ‘fine’ f and ‘coarse’ c nodes. The fine nodes are disconnected from the rest after dropping the $\mathcal{O}(\epsilon)$ terms. Hence, the degree of freedom in interface p has been reduced by $|f|$. The other interfaces can be sparsified similarly. The high-level view of the spaQR algorithm as described for square matrices in [16] is given in Algorithm 2.1.

Algorithm 2.1 High level spaQR algorithm

Require: Sparse matrix A , Maximum level L , Tolerance ϵ

- 1: Compute column and row partitioning of A , infer separators and interfaces
 - 2: **for all** $l = L, L - 1, \dots, 1$ **do**
 - 3: **for all** Interiors \mathcal{I} at level l **do**
 - 4: Factorize \mathcal{I} using block Householder reflections
 - 5: **end for**
 - 6: **for all** Interfaces \mathcal{S} between interiors **do**
 - 7: Scale the diagonal block corresponding to interface \mathcal{S}
 - 8: **end for**
 - 9: **for all** Interfaces \mathcal{S} between interiors **do**
 - 10: Sparsify \mathcal{S} using tolerance ϵ
 - 11: **end for**
 - 12: **end for**
-

2.2. Partitioning. We now explain our new algorithm emphasizing steps that are different from the algorithm for square matrices.

The vertex separators are obtained through a Nested Dissection partitioning on the graph of $A^T A$. This can be done either using a graph partitioning software like Metis or a hypergraph based partitioning like PaToH [43], hMetis [28] and Zoltan [8]. In our implementation, we provide the option partition using Metis [27] and PaToH [43]. Also, for problems where the underlying geometry is available, we can use it to efficiently partition the matrix. The quality of vertex separators and interfaces depend on the partitioning technique. Defining the ‘best’ technique is beyond the scope of this work.

Once we obtain the vertex separators, we can cluster the unknowns in the separator to define interfaces. We use the modified version of Nested Dissection described in [5] to do this. The idea is to keep track of the boundary \mathcal{B} of each interior \mathcal{I} and use this in the dissection process. One step of this scheme is shown in Figure 2. A detailed description of this scheme is given in Algorithm 2.2 of [5]. The columns of the matrix are reordered following the Nested Dissection ordering and the clustering hierarchy.

Least squares problems have more rows than columns. We want to assign rows to each column cluster such that the diagonal blocks in the reordered matrix will have a small condition number. Two strategies are used for the same. First, we perform a bipartite matching between the rows and columns of the matrix. This matches every column to a unique row of the matrix. The MC64 routine from the

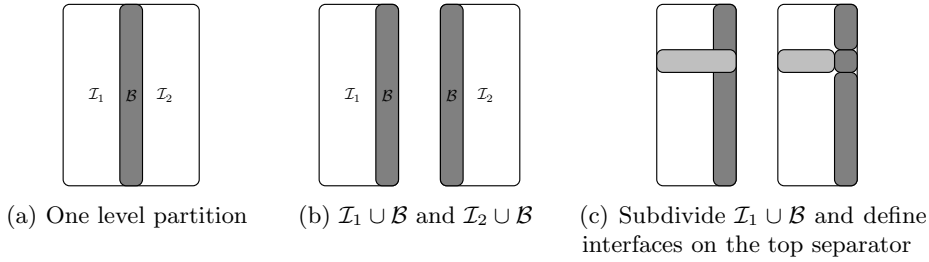


Fig. 2: The first figure shows a one level partition of an arbitrary graph (hypergraph) using nested dissection (HUND). The next two figures depict the process of identifying the interfaces by subdividing $\mathcal{I}_1 \cup \mathcal{B}$.

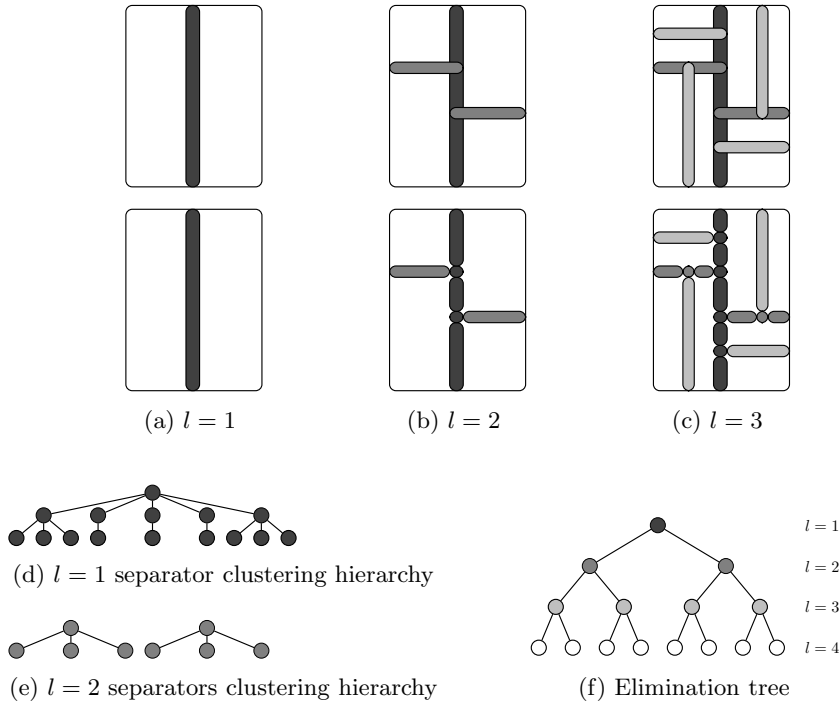


Fig. 3: (a), (b), (c) show the creation of separators and interfaces in the modified Nested Dissection algorithm. (d), (e) show the clustering hierarchy of the interfaces within each separator. (f) shows the elimination tree associated with the Nested Dissection partitioning.

HSL Mathematical Software Library [24] is used to perform the matching. This leaves us with $M - N$ unassigned rows. Each unassigned row r is assigned to cluster c such that, $c = \arg \max_{c_k} \sum_{j \in c_k} A_{r,j}^2$ where the summation is over all the nodes belonging to cluster c_k . This heuristic identifies the cluster such that the weight of the row is maximized in that cluster. We found that this heuristic works well in practice.

2.3. Householder QR on Separators. The factorization of separators at a level l is done by applying a block Householder step. Here, we describe the QR factorization of a separator s . Let s be the separator of interest, n be all its neighbors (i.e., $(A^T A)_{ns} \neq 0$) and w be the rest of the nodes disconnected from s in the graph of $A^T A$. Let nodes in n be further categorized into $n = \{n_1, n_2, n_3\}$. Nodes n_1 are such that $A_{n_1 s} \neq 0$, while A_{sn_1} may or may not be zero. Nodes n_2 are such that $A_{n_2 s} = 0$ and $A_{sn_2} \neq 0$ and nodes n_3 are such that $A_{n_1 n_3} \neq 0$ and $A_{sn_3} = 0$. All such nodes n will correspond to $(A^T A)_{ns} \neq 0$. Consider the matrix A blocked in the following form,

$$A = \begin{bmatrix} A_{ss} & A_{sn_1} & A_{sn_2} & & \\ A_{n_1 s} & A_{n_1 n_1} & & A_{n_1 n_3} & \\ & A_{n_2 n_2} & A_{n_2 n_3} & A_{n_2 w} & \\ & A_{n_3 n_1} & A_{n_3 n_2} & A_{n_3 n_3} & A_{n_3 w} \\ & A_{wn_1} & A_{wn_2} & A_{wn_3} & A_{ww} \end{bmatrix}$$

When dealing with tall thin matrices, the diagonal blocks corresponding to each separator/interior are also tall and thin. Let us denote the number of rows in a diagonal block A_{pp} as r_p and the number of columns as c_p . Then, the block Householder transformation H on the columns of separator s gives us,

$$H^T \begin{bmatrix} \boxed{A_{ss}} \\ \boxed{A_{n_1 s}} \end{bmatrix} = \begin{bmatrix} \boxed{\hat{R}_{ss}} \end{bmatrix} \text{ where, } \hat{R}_{ss} = \begin{bmatrix} \blacktriangledown \end{bmatrix}$$

Define,

$$H_s = \begin{bmatrix} H & \\ & I \end{bmatrix}$$

Then,

$$H_s^T A = \begin{bmatrix} \hat{R}_{ss} & \hat{R}_{sn_1} & \hat{R}_{sn_2} & \hat{R}_{sn_3} & \\ \hat{A}_{n_1 n_1} & \hat{A}_{n_1 n_2} & \hat{A}_{n_1 n_3} & & \\ & A_{n_2 n_2} & A_{n_2 n_3} & A_{n_2 w} & \\ & A_{n_3 n_1} & A_{n_3 n_2} & A_{n_3 n_3} & A_{n_3 w} \\ & A_{wn_1} & A_{wn_2} & A_{wn_3} & A_{ww} \end{bmatrix}$$

Note that each \hat{R}_{sn_i} block is rectangular of size $r_s \times c_{n_i}$. Only the top c_s rows go into the final R matrix. In the multifrontal QR, the extra $r_s - c_s$ rows below the main diagonal are added to the parent of s in the elimination tree. In our implementation, we split the extra rows between the clusters comprising n_1 (which can include any of the ancestors of s in the elimination tree), following the maximum norm heuristic outlined in [Subsection 2.2](#). Following this permutation, we have,

$$P_s^T H_s^T A = \begin{bmatrix} R_{ss} & R_{sn_1} & R_{sn_2} & R_{sn_3} & \\ & \tilde{A}_{n_1 n_1} & \tilde{A}_{n_1 n_2} & \tilde{A}_{n_1 n_3} & \\ & & A_{n_2 n_2} & A_{n_2 n_3} & A_{n_2 w} \\ & & A_{n_3 n_1} & A_{n_3 n_2} & A_{n_3 n_3} & A_{n_3 w} \\ & & A_{wn_1} & A_{wn_2} & A_{wn_3} & A_{ww} \end{bmatrix} = \begin{bmatrix} R_{ss} & R_{sn} & \\ & \tilde{A}_{nn} & A_{nw} \\ & A_{wn} & A_{ww} \end{bmatrix}$$

where, each R_{sn_i} block corresponds to the first s rows of the block \hat{R}_{sn_i} . The cluster s is now disconnected from the rest. We have only introduced fill-in between the

neighbors n and not affected the blocks involving w . Then we proceed by only focusing on the trailing matrix,

$$P_s^T H_s^T A R_s^{-1} = \begin{bmatrix} I_s & & \\ & \tilde{A}_{nn} & A_{nw} \\ & A_{wn} & A_{ww} \end{bmatrix}$$

where,

$$R_s = \begin{bmatrix} R_{ss} & R_{sn} & & \\ & I_n & & \\ & & & I_w \end{bmatrix}$$

2.4. Scaling of Interfaces. The spaQR algorithm performs a block diagonal scaling on all the remaining interfaces after every level of separator/interior factorization. This has been shown to improve the accuracy and performance of the preconditioner in solving linear systems. We perform a similar block diagonal scaling in solving linear least squares problems as well. Consider an interface p and its neighbors n ,

$$A = \begin{bmatrix} A_{pp} & A_{pn} \\ A_{np} & A_{nn} \end{bmatrix}$$

Let A_{pp} be a $r_p \times c_p$ block with $r_p \geq c_p$. Find the QR decomposition of A_{pp} ; $A_{pp} = U_{pp} R_p$, where $R_p = \begin{bmatrix} R_{pp} \\ 0 \end{bmatrix}$, $U_{pp} \in \mathbb{R}^{r_p \times r_p}$, and $R_{pp} \in \mathbb{R}^{c_p \times c_p}$. Then

$$U_{pp}^T A_{pp} R_p^{-1} = \bar{I}_p = \begin{bmatrix} I_{c_p} \\ 0 \end{bmatrix}$$

Define,

$$U_p = \begin{bmatrix} U_{pp} & \\ & I_{r_n} \end{bmatrix} \quad R_p = \begin{bmatrix} R_{pp} & \\ & I_{c_n} \end{bmatrix}$$

Then,

$$U_p^T A R_p^{-1} = \begin{bmatrix} I_{c_p} & \tilde{A}_{p_1 n} \\ 0 & \tilde{A}_{p_2 n} \\ \tilde{A}_{np} & A_{nn} \end{bmatrix}$$

where $U_{pp}^T A_{np} = \begin{bmatrix} \tilde{A}_{p_1 n} \\ \tilde{A}_{p_2 n} \end{bmatrix}$ and $A_{p_1 n}$ is $c_p \times c_n$ matrix. Similarly we scale the diagonal blocks belonging to the other interfaces.

2.5. Sparsification of Interfaces. Once the separators/interiors at a level l have been factorized and the remaining interfaces scaled, the final step is sparsification. This is different from the interface sparsification described for square matrices in [16].

The sparsification of the interfaces is done in two step as described next. Consider an interface p (after block diagonal scaling) and the associated block matrix,

$$A = \begin{bmatrix} I_{c_p} & A_{p_1 n} & & \\ 0 & A_{p_2 n} & & \\ A_{np} & A_{nn} & A_{nw} & \\ & A_{wn} & A_{ww} & \end{bmatrix}$$

Assume the off-diagonal blocks A_{np} , $A_{p_1 n}$ and $A_{p_2 n}$ are low-rank.

2.5.1. Step 1: Compress rows $A_{p_2 n}$. Consider a low rank approximation of $A_{p_2 n}$ as follows,

$$A_{p_2 n} = Q'_{pp} W'_{pn} = [Q'_{pc} \quad Q'_{pf}] \begin{bmatrix} W'_{cn} \\ W'_{fn} \end{bmatrix} \quad \text{with} \quad \|W'_{fn}\|_2 = \mathcal{O}(\epsilon)$$

Define Q'_p as,

$$Q'_p = \begin{bmatrix} I & & \\ & Q'_{pp} & \\ & & I \end{bmatrix}$$

to get,

$$(Q'_p)^T A = \begin{bmatrix} I_{c_p} & A_{p_1 n} & & \\ & W'_{cn} & & \\ & W'_{fn} & & \\ A_{np} & A_{nn} & A_{nw} & \\ & A_{wn} & A_{ww} & \end{bmatrix}$$

The block $\|W'_{fn}\| = \mathcal{O}(\epsilon)$ and the corresponding rows can be ignored. This step is not necessary in the spaQR factorization of square matrices. However, for least squares systems, this step keeps the aspect ratio of the diagonal blocks bounded throughout the algorithm. A bounded aspect ratio is important to ensure a linear complexity as we will show in [Section 3](#).

2.5.2.]. Step 2: Compress block $[A_{np}^T \quad A_{p_1 n}]$
Consider a low rank approximation of,

$$[A_{np}^T \quad A_{p_1 n}] = Q_{pp} W_{pn} = [Q_{pf} \quad Q_{pc}] \begin{bmatrix} W_{fn} \\ W_{cn} \end{bmatrix} \quad \text{with} \quad \|W_{fn}\|_2 = \mathcal{O}(\epsilon)$$

$$\begin{bmatrix} W_{fn} \\ W_{cn} \end{bmatrix} = \begin{bmatrix} W_{fn}^{(1)} & W_{fn}^{(2)} \\ W_{cn}^{(1)} & W_{cn}^{(2)} \end{bmatrix}$$

Define,

$$Q_p = \begin{bmatrix} Q_{pp} & \\ & I \end{bmatrix}$$

to get,

$$Q_p^T A Q_p = \begin{bmatrix} I_f & & E_2 & & \\ & I_c & W_{cn}^{(2)} & & \\ & & W'_{cn} & & \\ E_1 & W_{cn}^{(1)T} & A_{nn} & A_{nw} & \\ & & A_{wn} & A_{ww} & \end{bmatrix}$$

where $E_1 = W_{fn}^{(1)T}$, $E_2 = W_{fn}^{(2)}$ and $\|E_1\|_2 \approx \|E_2\|_2 \leq \epsilon$.

The spaQR for square matrices sparsifies the interfaces by performing only the second step shown here. However, the first step is crucial for tall, thin matrices. In practice, we perform step 1 on all remaining interfaces at a given l and then perform step 2. This is in contrast to performing step 1 and step 2 on a particular interface before moving on to the next interface. This approach is more expensive as the size of A_{np} block for some interface p can be bigger (when the rows below the diagonal of n have not been sparsified yet).

After sparsification, we can proceed by focusing on the trailing matrix,

$$Q_p^T(Q'_p)^T A Q_p = \begin{bmatrix} I_f & & & \\ & \tilde{A}_{cc} & \tilde{A}_{cn} & \\ & \tilde{A}_{nc} & A_{nn} & A_{nw} \\ & & A_{wn} & A_{ww} \end{bmatrix}$$

where $\tilde{A}_{cc} = \begin{bmatrix} I_c \\ 0 \end{bmatrix}$, $\tilde{A}_{cn} = \begin{bmatrix} W_{cn}^{(2)} \\ W'_{cn} \end{bmatrix}$ and $\tilde{A}_{nc} = W_{cn}^{(1)T}$. In this process, we have disconnected f from the rest and decreased the size of interface p by $|f|$. The $n - n$, $n - w$, $w - w$ edges are not affected. In [16], we give a detailed proof to show that sparsification does not affect the elimination tree of $A^T A$, that is, any two disjoint subtrees remain disjoint after sparsification. We claim that the same argument still holds and can be shown by following the exact steps given in Appendix C of [16].

2.6. Merging of clusters. Once the factorization of separators at a level is done, the interfaces of the remaining ND separators are merged following the cluster hierarchy. For example, in Figure 3, once the leaves $l = 4$ and the $l = 3$ separators are factorized, the interfaces of the separators at $l = 1, 2$ are merged following the clustering hierarchy shown in Figures 3d and 3e. Merging simply means combining the block rows and columns of the interfaces into a single block matrix.

2.7. Sparsified QR. We can now explain the complete modified spaQR algorithm for rectangular (tall, thin) matrices. First, we scale the columns of the matrix, so that the 2-norm of each column is a constant. Next, we obtain vertex separators and interfaces by partitioning the matrix using Metis or PaToH. This gives us a reordering for the columns of the matrix. Finally, we find a good row permutation by following the heuristics outlined in Subsection 2.2. Then, we apply our hierarchical solver, spaQR, to factorize the reordered matrix. The modified spaQR algorithm performs the following sequence of operations at every level l in the elimination tree: block Householder factorizations (H_s, R_s) on the interiors/separators (see Subsection 2.3), reassigning the rows below the diagonal of each factorized interior/separator P_s (see Subsection 2.3), interface scaling (U_p, R_p) (see Subsection 2.4), interface sparsification (Q'_p, Q_p) (see Subsection 2.5) (including some permutations to move the fine nodes and merging of the clusters (see Subsection 2.6)). This leads to a factorization of the form,

$$Q^T A W^{-1} \approx I$$

where,

$$Q = \prod_{l=1}^L \left(\prod_{s \in S_l} H_s P_s \prod_{p \in C_l} U_p \prod_{p \in C_l} Q'_p \prod_{p \in C_l} Q_p \right)$$

$$W = \prod_{l=L}^1 \left(\prod_{p \in C_l} Q_p^T \prod_{p \in C_l} R_p \prod_{s \in S_l} R_s \right)$$

Here, S_l is the set of all separators at level l in the elimination tree and C_l is the set of all interfaces remaining after factorization of separators at level l . Q is a product of orthogonal matrices and W is a product of upper triangular and orthogonal matrices. Since, Q and W are available as sequence of elementary transformations, they are easy to invert. The complete algorithm is presented in Algorithm 2.2.

Algorithm 2.2 Sparsified QR (spaQR) algorithm

Require: Sparse matrix A , Tolerance ϵ

- 1: Compute column and row partitioning of A , infer separators and interfaces (see [Subsection 2.2](#))
 - 2: **for all** $l = L, L - 1, \dots, 1$ **do**
 - 3: **for all** separators s at level l **do**
 - 4: Factorize s using block Householder (see [Subsection 2.3](#))
 - 5: Append H_s to Q and R_s to W
 - 6: Reassign the rows in s below the diagonal to other neighbor interfaces (see [Subsection 2.3](#))
 - 7: Append P_s to Q
 - 8: **end for**
 - 9: **for all** interfaces p remaining at level l **do**
 - 10: Perform block diagonal scaling on p (see [Subsection 2.4](#))
 - 11: Append U_p to Q and R_p to W
 - 12: **end for**
 - 13: **for all** interfaces p remaining at level l **do**
 - 14: Sparsify interface p by performing step 1 of the sparsification process (see [Subsection 2.5.1](#))
 - 15: Append Q'_p to Q
 - 16: **end for**
 - 17: **for all** interfaces p remaining at level l **do**
 - 18: Sparsify interface p by performing step 2 of the sparsification process (see [Subsection 2.5.2](#))
 - 19: Append Q_p to Q and Q_p^T to W
 - 20: **end for**
 - 21: **for all** separators s remaining at level l **do**
 - 22: Merge interfaces of s one level following the cluster hierarchy (see [Subsection 2.6](#))
 - 23: **end for**
 - 24: **end for**
 - 25: **return** $Q = \prod_{l=1}^L \left(\prod_{s \in S_l} H_s P_s \prod_{p \in C_l} U_p \prod_{p \in C_l} Q'_p \prod_{p \in C_l} Q_p \right)$
 $W = \prod_{l=L}^1 \left(\prod_{p \in C_l} Q_p^T \prod_{p \in C_l} R_p \prod_{s \in S_l} R_s \right)$ such that $Q^T A W^{-1} \approx I$
-

3. Complexity analysis. In [16], we discussed the complexity of the spaQR algorithm for square matrices under some assumptions. Let us now discuss the complexity for matrices with aspect ratio $\alpha > 1$ under the same assumptions. Consider the Nested Dissection process on the graph of $A^T A$ ($G_{A^T A}$). Let us define a node as a subgraph of $G_{A^T A}$. The root of the tree corresponds to $l = 1$ and the root node is the entire graph $G_{A^T A}$. The children nodes are subgraphs of $G_{A^T A}$ disconnected by a separator.

Let us write down the assumptions used in [16].

1. The leaf nodes in the elimination tree contain at most N_0 nodes, where $N_0 \in \mathcal{O}(1)$.
2. Let D_i be the set of all nodes j that are descendants of a node i , whose size is

at least $n_i/2$. We assume that the size of D_i is bounded, that is, $|D_i| = \mathcal{O}(1)$ for all i .

3. All the Nested Dissection separators are minimal. That is, every vertex in the separator is connected to two disconnected nodes in $G_{A^T A}$.
4. The number of edges leaving a node (subgraph) of size n_i is at most $n_i^{2/3}$. In other words, a node of size n_i is connected to at most $n_i^{2/3}$ vertices in $G_{A^T A}$. Most matrices that arise in the discretization of 2D and 3D PDEs satisfy this property.

Multifrontal QR. We first estimate the cost of multifrontal QR on sparse matrices under our assumptions. Consider matrix A of size $M \times N$, $\alpha = M/N$, obtained from a PDE discretization on a 3D grid (for example, matrices obtained from PDE constrained optimization problems as shown in [Subsection 4.1.2](#)). The node at the top of the elimination tree has a size of N . By assumption 4, the associated separator has size of,

$$c_{\text{top}} \in \mathcal{O}(N^{2/3})$$

The cost of Householder QR on the block corresponding to the last separator is $\mathcal{O}(r_l c_l^2)$ where r_l is the number of rows in the separator block. At the time of factorization of the top separator,

$$r_{\text{top}} \in \mathcal{O}((\alpha - 1)N + N^{2/3})$$

as all the extra rows of other separators get moved to the end. Then, the cost of factorizing the top separator block is,

$$h_{\text{top}} = \mathcal{O}((\alpha - 1)N^{7/3} + N^2)$$

The total cost of the multifrontal QR on the matrix is at least h_{top}

$$t_{\text{QR, fact}} = \Omega((\alpha - 1)N^{7/3} + N^2) \quad (\text{the notation } \Omega \text{ means bounded from below})$$

Next, we estimate the cost of applying the factorization to a vector $b \in \mathbb{R}^M$. Assume that we are using the corrected seminormal equations approach [3] which involves solving $R^T R x = A^T b$. Thus, we need to evaluate the cost of solving a linear system with R and R^T . A node i at a level l in the elimination tree is of size $2^{-l+1}N \leq n_i \leq 2^{-l+2}N$. The associated separator has a size of at most $\mathcal{O}(n_i^{2/3})$ and $\mathcal{O}(n_i^{2/3})$ non-zeros per row. Then the cost of solving a linear system with R and R^T is,

$$t_{\text{QR, apply}} \in \mathcal{O}\left(\sum_{l=1}^L 2^l \left(2^{-2l/3} N^{2/3}\right)^2\right) = \mathcal{O}(N^{4/3})$$

spaQR. Let us now estimate the complexity of the spaQR factorization, by making additional assumptions on the sparsification process.

5. Sparsification reduces the size of an interface at level l to,

$$c'_l \in \mathcal{O}(2^{-l/3} N^{1/3})$$

This means that the rank scales roughly as the diameter of the separator.

6. An interface has $\mathcal{O}(1)$ neighbor interfaces
7. The aspect ratio of the diagonal blocks corresponding to each interface is $\Theta(\alpha)$. This implies that the number of rows of an interface at level l is,

$$r'_l \in \mathcal{O}(\alpha 2^{-l/3} N^{1/3})$$

Assumption 5 is a consequence of low rank interactions between separators that are far away in $G_{A^T A}$. This is comparable to complexity assumptions in the fast multipole method [19, 20], spaND [5], and HIF [23]. Assumption 7 is a consequence of the extra sparsification step defined in Subsection 2.5.

The fill-in in the sparsified QR process results in at most $\mathcal{O}(2^{-l/3}N^{1/3})$ entries in each row and column. This is in part due to the assumption on the size of the interfaces, the number of neighbor interfaces and the fact that new connections are only made between distance 1 neighbors of a node in $G_{A^T A}$.

The cost of the spaQR factorization is split into four parts:

- *Householder QR on interiors and separators.* A separator block has c'_l columns and r'_l rows right before it is factorized. Further, it has at most $\mathcal{O}(2^{-l/3}N^{1/3})$ non-zeros per row/column and $\mathcal{O}(1)$ neighbor interfaces. Then, the cost of doing QR on a separator is

$$h'_l \in \mathcal{O}(\alpha(2^{-l/3}N^{1/3})^3) = \mathcal{O}(2^{-l}N)$$

- *Scaling of interfaces.* The cost of scaling (QR on a block of size $r'_l \times c'_l$) an interface is $\mathcal{O}(\alpha 2^{-l}N)$.
- *Sparsification of interfaces: Step 1* The rows below the diagonal of each remaining interface are sparsified in the first step of the sparsification stage. In this step, we perform a rank-revealing QR on a block with $\mathcal{O}((\alpha - 1)c'_l)$ rows and $\mathcal{O}(n_{\text{nbr}}c'_l)$ columns, where n_{nbr} is the number of neighbor interfaces. We have assumed that the number of neighbor interfaces are $\mathcal{O}(1)$. Hence, for large α , the cost of sparsifying the rows below the diagonal of an interface is,

$$e'_l \in \mathcal{O}((\alpha - 1)(2^{-l/3}N^{1/3})^3) = \mathcal{O}(\alpha 2^{-l}N)$$

- *Sparsification of interfaces: Step 2* In this step, we compute a rank-revealing QR on the block $[A_{np}^T \ A_{p1n}]$. The cost of rank-revealing QR is $\mathcal{O}(mnr)$ where $r \leq \min(m, n)$. The number of rows of this block is c'_l . The number of columns is $\mathcal{O}(\alpha 2^{-l/3}N^{1/3})$ due to our assumptions on the size of the interface and the number of neighbor interfaces. Thus, this step costs,

$$s'_l \in \mathcal{O}(\alpha(2^{-l/3}N^{1/3})^3) = \mathcal{O}(\alpha 2^{-l}N)$$

Hence, the total cost of the spaQR algorithm is,

$$\begin{aligned} t_{\text{spaQR}} &\in \mathcal{O}\left(\sum_{l=1}^L \alpha 2^l 2^{-l} N\right) = \mathcal{O}\left(\sum_{l=1}^L \alpha N\right) \\ &= \mathcal{O}(\alpha N \log N), \quad L \in \Theta(\log(N/N_0)) \\ &= \mathcal{O}(M \log N) \end{aligned}$$

The cost of applying the factorization can be derived similarly to the analysis for the multifrontal QR algorithm. Solving the least squares system consists essentially in solving $W^T W x = A^T b$, where W is a sequence of sparse orthogonal and upper-triangular matrices. Using our assumption on the size of the interfaces, the total cost of applying the spaQR factorization is,

$$t_{\text{spaQR, apply}} \in \mathcal{O}\left(\sum_{l=1}^L \alpha 2^l \left(2^{-l/3}N^{1/3}\right)^2\right) = \mathcal{O}(\alpha N) = \mathcal{O}(M)$$

The memory required to store the factorization scales as the cost of applying the factorization. Hence,

$$\text{mem}_{\text{spaQR}} = \mathcal{O}(M)$$

We show numerical results in [Subsection 4.2](#) that corroborate the assumptions made here.

4. Benchmarks. In this section, we benchmark the performance of the algorithm for solving sparse linear least squares problem arising in various applications. First, we study the performance of the algorithm on matrices coming out of PDE constrained optimization on uniform 2D and 3D grids. We use a regular geometric partitioning on $A^T A$ to get the separators and infer the interfaces as outlined in [Subsection 2.2](#). Next, we study the performance on non-regular problems obtained from the Suite Sparse Matrix Collection. The Nested dissection partitioning is done using Metis on $A^T A$ or PaToH on A .

The spaQR algorithm is used to compute an approximate factorization using a user-defined tolerance ϵ . The approximate factorization is then used as a preconditioner with the CGLS (also known as CGNR) iterative solver. The convergence criteria is set as $\|A^T(Ax - b)\|_2 / \|A^T b\|_2 \leq 10^{-12}$. CGLS is based on solving the normal equations using Conjugate Gradient. Hence, the orthogonal factors that is applied on the left of the matrix need not be applied to the right hand side (we compute $A^T b$ in advance). Thus, we can further reduce the memory footprint by not storing the orthogonal factors that only operate on the left of the matrix.

The code was written in C++. We use GCC 8.1.0 and Intel(R) MKL 2019 for Linux for the BLAS and LAPACK operations. The number of levels in the nested dissection process is chosen as $\lceil \log(N/64) / \log 2 \rceil$ for a matrix of size $M \times N$. Low rank approximations are performed using LAPACK's `dlaqps` routine which performs a column pivoted QR on r columns. The value r is chosen such that $\frac{|R_{ii}|}{|R_{11}|} \geq \epsilon$ for $1 \leq i \leq r$, where R is the upper triangular matrix that comes out of the column pivoted QR method. We typically begin sparsification on levels 3 or 4.

4.1. Scaling with problem size. First, we study the performance of the algorithm with increasing problem size on the Inverse Poisson problem defined on uniform 2D and 3D grids.

4.1.1. 2D Inverse Poisson problem. Consider the following PDE-constrained optimization problem,

$$\begin{aligned} \min_{u,z} \quad & \frac{1}{2} \int_{\Omega} (u - u_d)^2 dx + \frac{1}{2} \lambda \int_{\Omega} z^2 dx \\ \text{subject to} \quad & -\nabla \cdot (z \nabla u) = h \text{ in } \Omega \\ & u = 0 \text{ in } d\Omega \end{aligned}$$

We want to recover the variables u and the diffusion coefficients z at every grid point on the 2D $n \times n$ grid, using the available observed states u_d .

One approach to solving this optimization problem [9] involves solving the least squares problem,

$$J^T x = b$$

where J is the Jacobian of the discretized constraints. The Jacobian can be written as $J = [J_u \ J_z]$ where the columns of J_u (resp. J_z) correspond to a partial derivative with respect to one of the u_i (z_i) variables. The Jacobian J can be evaluated with different values of (u, z) .

There are $N = n^2$ constraints as the PDE needs to be satisfied at every grid point and $M = n_u + n_z$ variables, where $n_u = n^2$ and $n_z = (n + 1)^2$. Generally speaking, if we choose random values for u and z we will get a least squares matrix (J^T) with an aspect ratio of 2. It is possible to reduce the aspect ratio of the matrix by artificially creating rows that are equal to 0. Then, by removing zero rows, we can reduce the aspect ratio of matrix A . A detailed explanation of the process of generating matrices with different aspect ratio is given in [Appendix A.1](#). In our benchmark, we considered aspect ratios equal to $\approx 2, 1.5,$ and 1.05 .

The results for the 2D Inverse Poisson problem are shown in [Figure 4](#); the number of columns are $N = n^2$ and the number of rows are $M = \alpha N$, with the aspect ratio α varying from 1.05 to 2. For small enough ϵ , the number of CGLS iterations needed to converge increase slowly with increasing problem size. We note that for problems with $\alpha \approx 1.05$, we need a smaller value of ϵ (10^{-4}) for good convergence, as these problems are ill-conditioned.

In the case of direct multifrontal QR (with the same nested dissection ordering), the size of the top separator will be $\mathcal{O}(N^{1/2})$. As more and more fill-in are introduced as the factorization proceeds, the block corresponding to the top separator will be dense when we reach the top of the elimination tree. The size of the top separator block will be of size $\mathcal{O}((\alpha - 1)N + N^{1/2}) \times \mathcal{O}(N^{1/2})$ and a Householder QR on this block will cost $\mathcal{O}((\alpha - 1)N^2 + N^{3/2})$ flops. On the other hand, the factorization time in spaQR scales as $\mathcal{O}(N)$ for all three values of α as expected. This is verified numerically and shown in [Figure 4](#).

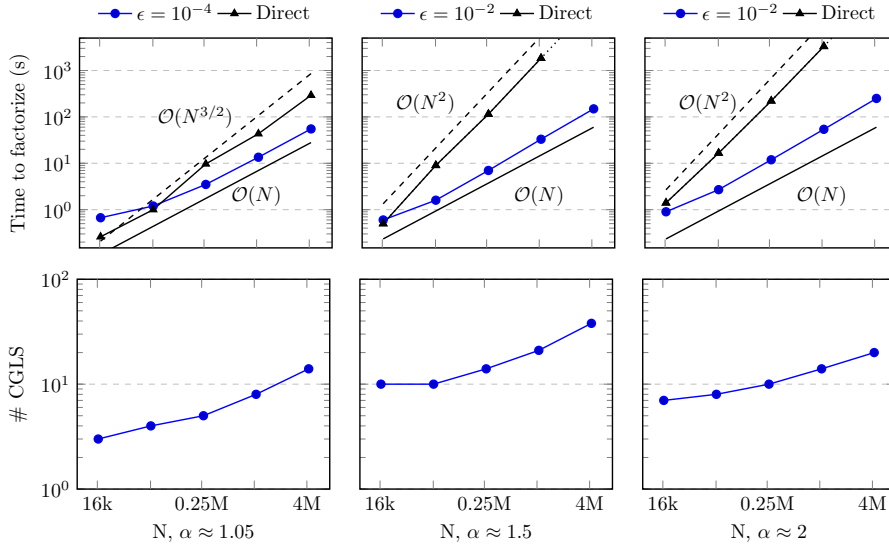


Fig. 4: Results for a 2D Inverse Poisson least squares problem for varying values of the aspect ratio $\alpha = M/N$. For small enough values of ϵ , the iteration counts increase slowly. Note that for smaller aspect ratio, the condition number is higher and hence requires a higher accuracy (smaller ϵ) to converge in < 50 iterations. The factorization time scales as $\mathcal{O}(N)$ for all three values of α .

We also compare the convergence of the CGLS residual with a diagonal preconditioner and using spaQR as the preconditioner. In [Figure 5](#), we show the convergence

results for the least squares problem on a 2048×2048 grid for three values of the aspect ratio α . In all three cases, the spaQR preconditioned CGLS takes less than 30 iterations to converge to a residual of 10^{-12} . However, the diagonal preconditioner performs poorly, taking around 100 iterations to reach a residual of 10^{-2} .

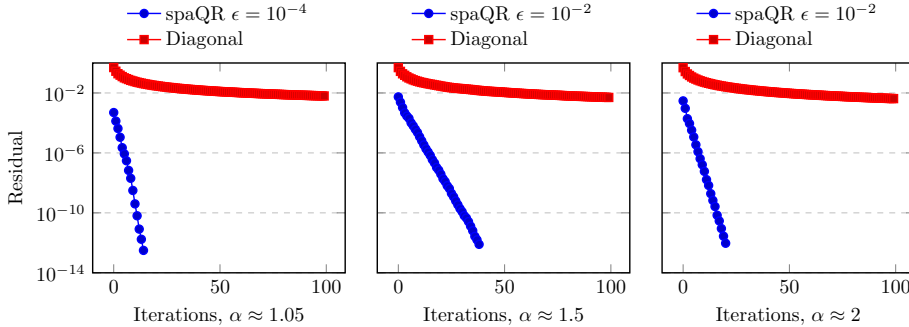


Fig. 5: Convergence of the residual $\|A^T(Ax - b)\|_2 / \|A^T b\|_2$ with the number of CGLS iterations with the diagonal preconditioner and spaQR for the 2048×2048 2D Inverse Poisson problem. Note the superiority of CGLS preconditioned with the spaQR method for all three values of the aspect ratio α .

4.1.2. 3D Inverse Poisson problem. Now consider the same problem defined on a uniform $n \times n \times n$ three-dimensional grid. There are $N = n^3$ constraints and $M = n_u + n_z$ variables, where $n_u = n^3$ and $n_z = (n + 1)^3$. Similar to the 2D problem, we discretize the variable coefficient Poisson equation using a finite difference scheme on a staggered grid. We are interested in the least squares problem obtained from the Jacobian of the discretized equations. As with the 2D case, by picking specific values for u we can create zero rows in A and as a result change the effective aspect ratio of the matrix. The matrix generation process is described in [Appendix B](#). In our benchmarks, we generate least squares problem of size $M \times N$, where $M = \alpha N$, $N = n^3$ and $\alpha \in \{1.05, 1.5, 2\}$.

[Figure 6](#) shows the number of CGLS iterations to converge and the time of factorization for the Inverse Poisson problem on a 3D grid. Theoretically, we expect the factorization time to scale as $\mathcal{O}(N \log N)$ for a fixed value of α (see [Section 3](#)). However, the empirical cost of factorization is $\mathcal{O}(N^{1.45})$. Based on other benchmarks, we believe this is due to non-asymptotic effects (e.g., terms in the computational runtime that vanish asymptotically but may dominate at small sizes). The number of iterations increases slowly (almost a constant for $\alpha = 1.5, 2$) for the range of problems considered. In [Figure 7](#) we compare the performance of CGLS with a standard diagonal preconditioner and spaQR. These results show the superior performance of spaQR as compared to some of the standard techniques in this area.

4.2. Profiling. In this section, we try to understand the time and memory requirements of the spaQR algorithm. First, we show some experimental evidence to back up the assumptions made in the complexity analysis. Assumptions 1 to 6 are the same as the assumptions used to get the complexity estimate for squares matrices in [\[16\]](#) in which we also provide experimental evidence for them. [Figure 8](#) shows that the aspect ratio of the diagonal blocks is almost a constant at each level in the elimination tree and is bounded by $\Theta(\alpha)$ at every level.

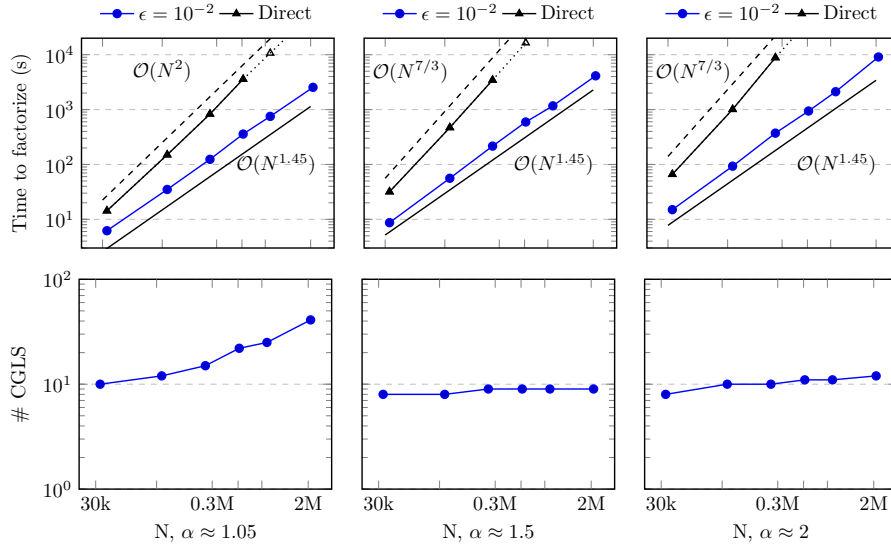


Fig. 6: Results of 3D Inverse Poisson least squares problem for varying values of aspect ratio, $\alpha = M/N$. For small enough values of ϵ , the iteration counts increase slowly. Empirically, the number of flops roughly scales as $\mathcal{O}(N^{1.45})$ for the values of α considered. The direct multifrontal QR scales like $\mathcal{O}((\alpha - 1)N^{7/3} + N^2)$ as expected.

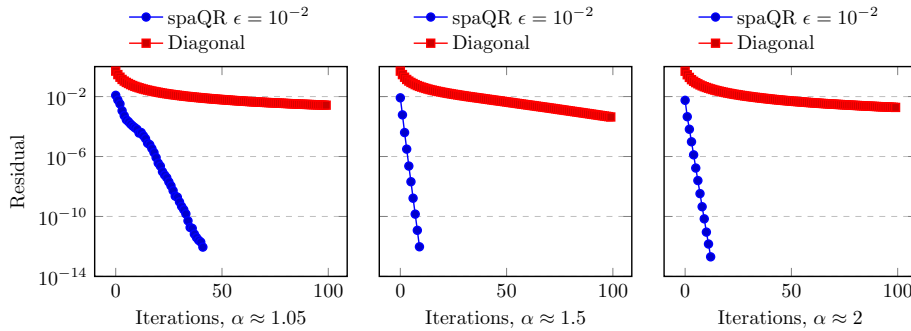


Fig. 7: Convergence of the residual $\|A^T(Ax - b)\|_2 / \|A^T b\|_2$ with the number of CGLS iterations with spaQR and a diagonal preconditioner for the $128 \times 128 \times 128$ 3D Inverse Poisson least squares problem. Note the superiority of CGLS preconditioned with the spaQR method for all three values of the aspect ratio α .

In Figure 9, we compare the size of the top separator with the problem size N . Note that for a fixed value of α , the size of the top separator grows as $\mathcal{O}(N^{1/3})$. Hence, the cost of factorizing the block matrix corresponding to the top separator is $\mathcal{O}(N)$. With $\Theta(\log(N/N_0))$ levels, the total cost of spaQR factorization is $\mathcal{O}(N \log N)$ for a fixed constant aspect ratio α . For more detailed complexity analysis, see Section 3. The memory needed to store the preconditioner scales as $\mathcal{O}(N)$. Empirically, we see that the scaling is $\mathcal{O}(N^{1.18})$, which may be due to non-asymptotic effects.

Figure 10 shows the runtime per level of the spaQR algorithm split into the

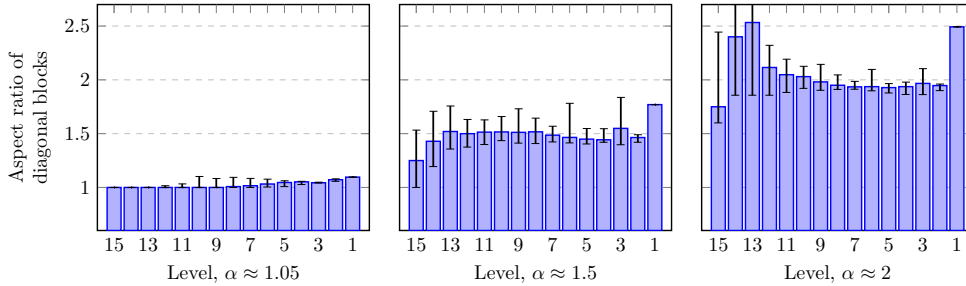


Fig. 8: The median aspect ratio of the diagonal blocks corresponding to the interfaces per level for the 3D Inverse Poisson problem on $N = 128^3$. The error bars show the interquartile range.

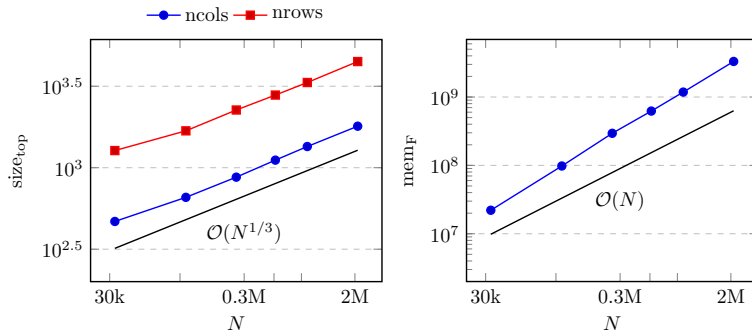


Fig. 9: The growth in the size of the top separator and the memory needed to store the preconditioner for the 3D Inverse Poisson problem with $\alpha \approx 2$.

different phases: factorize interiors/separators, sparsify the extra rows of each interior/separator and reassign them among its ancestors in the elimination tree, scale the interfaces, sparsify the interfaces and merge the clusters. We note that the time per level is roughly the same (a variation of around 6%) across level 10 to 7. As we scale to bigger problems, the small variations will not matter and we expect a constant runtime per level.

4.3. Non-regular problems. Next, we test our algorithm on the set of least-squares problems from the Suite Sparse Matrix Collection given in [Subsection 4.3](#). The matrix was partitioned using Metis [27] and the spaQR algorithm was run with a tolerance ϵ that is tuned for each problem. Two of the matrices, graphics and Hardesty3, proved the most challenging for spaQR, requiring a lower tolerance of $\epsilon = 10^{-4}$ and $\epsilon = 10^{-5}$ respectively. CGLS preconditioned with spaQR performed well for all the test matrices and converged in at most 25 iterations.

5. Conclusions. In this work, we extended the spaQR algorithm to solve large, sparse linear least squares problems. We introduced a two-step sparsification process to effectively sparsify the interfaces for tall and thin matrices. With this, we empirically showed that the aspect ratio of each diagonal block remains bounded and lead to a $\mathcal{O}(M \log N)$ runtime for the algorithm. We numerically benchmarked our

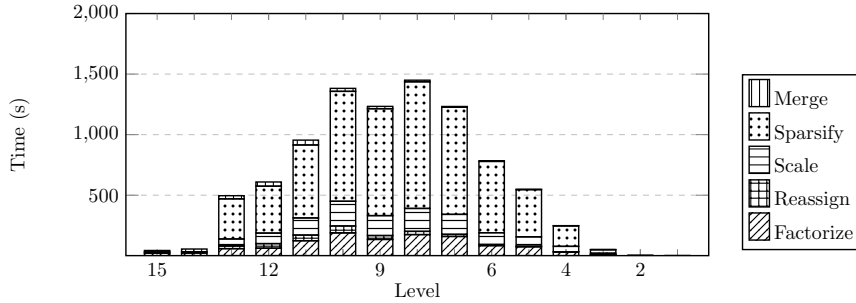


Fig. 10: The runtime per level of the spaQR algorithm split into the five phases: factorize interiors/separators, reassign rows below the diagonal of each factorized interior/separator, scale interfaces, sparsify interfaces, and merge the clusters. We skip sparsification for two levels. The results are shown for the 3D Inverse Poisson problem with $N = 128^3$ and $\alpha \approx 2$.

Table 1: List of test matrices and their properties: number of rows and columns (nrows, ncols), aspect ratio(α), number of non-zeros (nnz), condition number (cond. no.)

| Matrix | nrows | ncols | α | nnz | cond. no. |
|--------------|-----------|-----------|----------|------------|--------------------|
| mesh_deform | 234,023 | 9,393 | 24.9 | 853,829 | 1.16×10^3 |
| Kemelmacher | 28,452 | 9,693 | 2.9 | 10,0875 | 2.4×10^4 |
| human | 20,000 | 10,198 | 1.9 | 119,952 | - |
| graphics | 29,493 | 11,822 | 2.5 | 117,954 | 1.6×10^8 |
| image_interp | 240,000 | 120,000 | 2.0 | 711,683 | - |
| Hardesty2 | 929,901 | 303,645 | 3.1 | 4,020,731 | - |
| Hardesty3 | 8,217,820 | 7,591,564 | 1.1 | 40,451,632 | - |

Table 2: Performance of spaQR on some Suite Sparse matrices: tolerance set (ϵ), time to partition, factorize, solve (t_P , t_F , t_S), number of CGLS iterations (#CGLS), size of the top separator ($size_{top}$), memory required to store the preconditioner (mem_F)

| Matrix | ϵ | t_P (s) | t_F (s) | t_S (s) | #CGLS | $size_{top}$ (n_{rows}, n_{cols}) | mem_F (10^8) |
|--------------|------------|--------------|--------------|--------------|-------|--|-----------------------|
| mesh_deform | 10^{-2} | 0.39 | 1.38 | 0.27 | 8 | (648, 55) | 0.006 |
| Kemelmacher | 10^{-2} | 0.08 | 0.64 | 0.25 | 20 | (82, 22) | 0.011 |
| human | 10^{-2} | 0.08 | 0.28 | 0.23 | 25 | (285, 58) | 0.006 |
| graphics | 10^{-4} | 0.07 | 0.25 | 0.13 | 17 | (449, 90) | 0.005 |
| image_interp | 10^{-3} | 0.92 | 5.46 | 1.12 | 8 | (7977, 130) | 0.131 |
| Hardesty2 | 10^{-3} | 3.90 | 13.5 | 12.8 | 24 | (207, 73) | 0.289 |
| Hardesty3 | 10^{-5} | 96.1 | 384 | 165 | 10 | (586, 226) | 11.52 |

algorithm by testing on large sparse least squares problem arising in optimization problems and other non-regular problems from the Suite Sparse Matrix Collection [7]. The numerical tests showed the superiority of spaQR over direct multifrontal QR and CGLS iterative method with a standard diagonal preconditioner.

With this extension to solving large sparse least squares problems, the spaQR solver opens up new applications of low-rank approximations to many areas of computational science. One such area that was investigated in this work is constrained optimization problems. Other potential application domains are computational geometry and computer graphics. This will be investigated in a future work. While the current implementation is sequential, the organization of the algorithm naturally exhibits parallelism. This will be investigated in future research.

6. Acknowledgements. The computing for this project was performed on the Sherlock research cluster, hosted at Stanford University. We thank Stanford University and the Stanford Research Computing Center for providing the computational resources and support that contributed to this research. This work was partly funded by a grant from Sandia National Laboratories (Laboratory Directed Research and Development [LDRD]) entitled “Hierarchical Low-rank Matrix Factorizations,” and a grant from the National Aeronautics and Space Administration (NASA, agreement #80NSSC18M0152). We thank Léopold Cambier, Erik G. Boman, Juan Alonso, Zan Xu, Jordi Feliu-Fàba and Steven Brill for valuable discussions. Finally, we also thank Ron Estrin for providing the PDE constrained optimization examples as a test case for our algorithm.

REFERENCES

- [1] P. R. AMESTOY, I. S. DUFF, J.-Y. L’EXCELLENT, AND J. KOSTER, *Mumps: A general purpose distributed memory sparse solver*, in Applied Parallel Computing. New Paradigms for HPC in Industry and Academia, T. Sørenvik, F. Manne, A. H. Gebremedhin, and R. Moe, eds., Berlin, Heidelberg, 2001, Springer Berlin Heidelberg, pp. 121–130.
- [2] P. BENNER AND T. MACH, *On the qr decomposition of h-matrices*, Computing, 88 (2010), <https://doi.org/10.1007/s00607-010-0087-y>.
- [3] A. BJÖRCK, *Stability analysis of the method of semi-normal equations for least squares problems*, Linear Algebra and its Applications, 88-89 (1987), pp. 31–48, [https://doi.org/10.1016/0024-3795\(87\)90101-7](https://doi.org/10.1016/0024-3795(87)90101-7).
- [4] Å. BJÖRCK, *Numerical methods for least square problems*, 1996.
- [5] L. CAMBIER, C. CHEN, E. BOMAN, S. RAJAMANICKAM, R. TUMINARO, AND E. DARVE, *An algebraic sparsified nested dissection algorithm using low-rank approximations*, SIAM Journal on Matrix Analysis and Applications, 41 (2020), pp. 715–746, <https://doi.org/10.1137/19M123806X>.
- [6] E. CHOW AND Y. SAAD, *Experimental study of ilu preconditioners for indefinite matrices*, Journal of Computational and Applied Mathematics, 86 (1997), pp. 387–414.
- [7] T. A. DAVIS AND Y. HU, *The university of florida sparse matrix collection*, ACM Trans. Math. Softw., 38 (2011), <https://doi.org/10.1145/2049662.2049663>, <https://doi.org/10.1145/2049662.2049663>.
- [8] K. D. DEVINE, E. G. BOMAN, R. T. HEAPHY, R. H. BISSELING, AND U. V. CATALYUREK, *Parallel hypergraph partitioning for scientific computing*, IEEE, 2006.
- [9] R. ESTRIN, M. P. FRIEDLANDER, D. ORBAN, AND M. A. SAUNDERS, *Implementing a smooth exact penalty function for equality-constrained nonlinear optimization*, 2019, <https://arxiv.org/abs/1910.04300>.
- [10] M. FAVERGE, G. PICHON, P. RAMET, AND J. ROMAN, *On the use of h-matrix arithmetic in pastix: a preliminary study*, in Workshop on Fast Solvers, Toulouse, France, June 2015, <http://www.labri.fr/~ramet/restricted/cimi15.pdf>.
- [11] J. FELIU-FABÀ, K. HO, AND L. YING, *Recursively preconditioned hierarchical interpolative factorization for elliptic partial differential equations*, Communications in Mathematical Sciences, 18 (2020), pp. 91–108, <https://doi.org/10.4310/CMS.2020.v18.n1.a4>.

- [12] J. FELIU-FABÀ AND L. YING, *Hierarchical interpolative factorization preconditioner for parabolic equations*, 2020, <https://arxiv.org/abs/2004.05566>.
- [13] D. C.-L. FONG AND M. A. SAUNDERS, *Lsmr: An iterative algorithm for sparse least-squares problems.*, SIAM J. Scientific Computing, 33 (2011), pp. 2950–2971, <http://dblp.uni-trier.de/db/journals/siamsc/siamsc33.html#FongS11>.
- [14] A. GEORGE, *Nested dissection of a regular finite element mesh*, SIAM Journal on Numerical Analysis, 10 (1973), pp. 345–363.
- [15] P. GHYSELS, X. S. LI, F.-H. ROUET, S. WILLIAMS, AND A. NAPOV, *An efficient multicore implementation of a novel hss-structured multifrontal solver using randomized sampling*, SIAM J. Scientific Computing, 38 (2016).
- [16] A. GNANASEKARAN AND E. DARVE, *Hierarchical orthogonal factorization: Sparse square matrices*, 2020, <https://arxiv.org/abs/2010.06807>.
- [17] G. H. GOLUB, *Numerical methods for solving linear least squares problems*, Numerische Mathematik, 7 (1965), pp. 206–216.
- [18] G. H. GOLUB AND C. F. VAN LOAN, *Matrix Computations (3rd Ed.)*, Johns Hopkins University Press, USA, 1996.
- [19] L. GREENGARD AND V. ROKHLIN, *A fast algorithm for particle simulations*, J. Comput. Phys., 135 (1997), p. 280–292, <https://doi.org/10.1006/jcph.1997.5706>, <https://doi.org/10.1006/jcph.1997.5706>.
- [20] L. GREENGARD AND V. ROKHLIN, *A new version of the fast multipole method for the laplace equation in three dimensions*, Acta Numerica, 6 (1997), p. 229–269, <https://doi.org/10.1017/S0962492900002725>.
- [21] M. R. HESTENES AND E. STIEFEL, *Methods of conjugate gradients for solving linear systems*, Journal of research of the National Bureau of Standards, 49 (1952), pp. 409–436.
- [22] K. L. HO AND L. YING, *Hierarchical interpolative factorization for elliptic operators: differential equations*, 2013, <https://arxiv.org/abs/1307.2895>.
- [23] K. L. HO AND L. YING, *Hierarchical interpolative factorization for elliptic operators: Integral equations*, 2016.
- [24] HSL(2013), *A collection of fortran codes for large scale scientific computation*, <http://www.hsl.rl.ac.uk>.
- [25] D. JAMES, *Conjugate gradient methods for constrained least squares problems*, 1990.
- [26] A. JENNINGS AND M. A. AJIZ, *Incomplete methods for solving $a^t a x = b$* , SIAM J. Sci. Stat. Comput., 5 (1984), p. 978–987, <https://doi.org/10.1137/0905067>, <https://doi.org/10.1137/0905067>.
- [27] G. KARYPIS AND V. KUMAR, *A fast and high quality multilevel scheme for partitioning irregular graphs*, SIAM J. Sci. Comput., 20 (1998), p. 359–392.
- [28] G. KARYPIS AND V. KUMAR, *Hmetis: a hypergraph partitioning package*, 1998.
- [29] B. KLOCKIEWICZ, L. CAMBIER, R. HUMBLE, H. TCHELEPI, AND E. DARVE, *Second order accurate hierarchical approximate factorization of sparse spd matrices*, 2020, <https://arxiv.org/abs/2007.00789>.
- [30] N. LI AND Y. SAAD, *Migr: A multilevel incomplete qr preconditioner for large sparse least-squares problems*, SIAM J. Matrix Analysis Applications, 28 (2006), pp. 524–550, <https://doi.org/10.1137/050633032>.
- [31] T. MANTEUFFEL, *An incomplete factorization technique for positive definite linear systems*, Mathematics of Computation, 34 (1980), pp. 473–497.
- [32] J. NAGEL AND N. ORG, *Solving the generalized poisson equation using the finite-difference method (fdm)*, (2011).
- [33] C. C. PAIGE AND M. A. SAUNDERS, *Lsqr: An algorithm for sparse linear equations and sparse least squares.*, ACM Trans. Math. Softw., 8 (1982), pp. 43–71, <http://dblp.uni-trier.de/db/journals/toms/toms8.html#PaigeS82>.
- [34] G. PICHON, E. DARVE, M. FAVERGE, P. RAMET, AND J. ROMAN, *Sparse supernodal solver using block low-rank compression*, in 2017 IEEE International Parallel and Distributed Processing Symposium Workshops (IPDPSW), 2017, pp. 1138–1147.
- [35] H. POURANSARI, P. COULIER, AND E. DARVE, *Fast hierarchical solvers for sparse matrices using extended sparsification and low-rank approximation*, SIAM Journal on Scientific Computing, 39 (2017), pp. A797–A830, <https://doi.org/10.1137/15M1046939>.
- [36] Y. SAAD, *Preconditioning techniques for nonsymmetric and indefinite linear systems*, 1988.
- [37] P. G. SCHMITZ AND L. YING, *A fast direct solver for elliptic problems on general meshes in 2d*, J. Comput. Phys., 231 (2012), pp. 1314–1338.
- [38] X. WANG, X. D., AND K. GALLIVAN, *Incomplete factorization preconditioning for linear least squares problems*, (2002).
- [39] Y. XI, J. XIA, S. CAULEY, AND V. BALAKRISHNAN, *Superfast and stable structured solvers for*

- toeplitz least squares via randomized sampling*, SIAM J. Matrix Analysis Applications, 35 (2014), pp. 44–72.
- [40] J. XIA, *Efficient structured multifrontal factorization for general large sparse matrices*, SIAM J. Scientific Computing, 35 (2013).
- [41] J. XIA, S. CHANDRASEKARAN, M. GU, AND X. S. LI, *Superfast multifrontal method for large structured linear systems of equations*, SIAM J. Matrix Analysis Applications, 31 (2009), pp. 1382–1411.
- [42] K. YANG, H. POURANSARI, AND E. DARVE, *Sparse hierarchical solvers with guaranteed convergence*, International Journal for Numerical Methods in Engineering, (2016), <https://doi.org/10.1002/nme.6166>.
- [43] Ü. V. ÇATALYÜREK AND C. AYKANAT, *Patoh (partitioning tool for hypergraphs)*, in Encyclopedia of Parallel Computing, 2011.

Appendix A. Matrix generation. Here, we provide a description of how to generate the least squares matrices used in the numerical experiments of the 2D and 3D Inverse Poisson problems.

A.1. 2D Inverse Poisson problem. Consider the variable coefficient Poisson equation,

$$\begin{aligned} -\nabla \cdot (z \nabla u) &= h \text{ in } \Omega \\ u &= 0 \text{ in } d\Omega \end{aligned}$$

discretized using finite difference on a staggered grid [32] shown in Figure 11. The discretization at grid point (i, j) is,

$$(A.1) \quad f(u, z) := -a_0 u_{i,j} + a_1 u_{i+1,j} + a_2 u_{i,j+1} + a_3 u_{i-1,j} + a_4 u_{i,j-1} + q_{i,j} = 0$$

where,

$$\begin{aligned} a_0 &= z_{i,j} + z_{i-1,j} + z_{i,j-1} + z_{i-1,j-1} \\ a_1 &= \frac{1}{2}(z_{i,j} + z_{i,j-1}) \\ a_2 &= \frac{1}{2}(z_{i-1,j} + z_{i,j}) \\ a_3 &= \frac{1}{2}(z_{i-1,j-1} + z_{i-1,j}) \\ a_4 &= \frac{1}{2}(z_{i,j-1} + z_{i-1,j-1}) \\ q_{i,j} &= \int_{\Omega_{ij}} h(r) d\Omega, \quad \Omega_{ij} \text{ is a square region around } u_{ij} \end{aligned}$$

The finite difference discretization leads to n^2 equations, one for each grid point on the 2D $n \times n$ grid. The number of variables is $n_u + n_z$, where $n_u = n^2$ and $n_z = (n+1)^2$. The Jacobian matrix is constructed by taking partial derivatives of each of the n^2 equations of the form Equation (A.1), with respect to each $u(i, j)$ and $z(i, j)$ variable. For example, the following are the partial derivatives of Equation (A.1),

$$\frac{\partial f}{\partial u_{i,j}} = -a_0 \quad \frac{\partial f}{\partial u_{i+1,j}} = a_1 \quad \frac{\partial f}{\partial u_{i,j+1}} = a_2 \quad \frac{\partial f}{\partial u_{i-1,j}} = a_3 \quad \frac{\partial f}{\partial u_{i,j-1}} = a_4$$

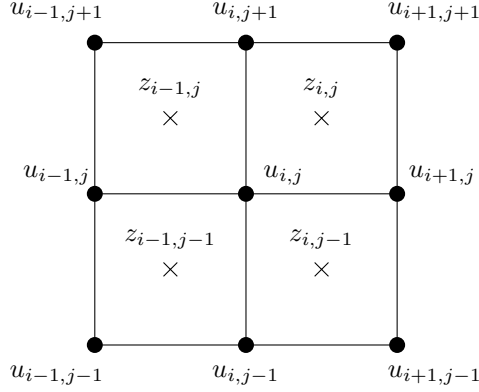


Fig. 11: Finite difference mesh for the 2D variable coefficient Poisson equation.

$$\begin{aligned} \frac{\partial f}{\partial z_{i,j}} &= -u_{i,j} + \frac{1}{2}u_{i+1,j} + \frac{1}{2}u_{i,j+1} \\ \frac{\partial f}{\partial z_{i-1,j}} &= -u_{i,j} + \frac{1}{2}u_{i,j+1} + \frac{1}{2}u_{i-1,j} \\ \frac{\partial f}{\partial z_{i,j-1}} &= -u_{i,j} + \frac{1}{2}u_{i+1,j} + \frac{1}{2}u_{i,j-1} \\ \frac{\partial f}{\partial z_{i-1,j-1}} &= -u_{i,j} + \frac{1}{2}u_{i-1,j} + \frac{1}{2}u_{i,j-1} \end{aligned}$$

We can evaluate the Jacobian at random values of u, z . Then, we solve the least squares problem, $J^T x = b$. In general, choosing random values of u, z leads to J^T having an aspect ratio of 2. It is possible to reduce the aspect ratio of the matrix by artificially creating rows that are equal to 0. This is done by choosing values for u such that u is constant in some region, say $u = 1$ in some region of the mesh. In that case, Equation (A.1) simplifies and the entire row become zero. Then, by removing zero rows, we can reduce the aspect ratio of matrix J^T .

For example, setting $u = 1$ and $z = 1$ everywhere on the grid (except the boundary where $u = 0$) will make most of the partial derivatives with respect to z variables zero (except the z variables near the boundary of the mesh). This leads to zero rows in J^T which can be removed to get an aspect ratio close to 1 for J^T .

Appendix B. 3D Inverse Poisson problem.

The finite difference discretization for the variable coefficient Poisson equation in a 3D $n \times n \times n$ mesh is as follows. At grid point (i, j) ,

$$(B.1) \quad \begin{aligned} f(u, z) := & -a_0 u_{i,j,k} + a_1 u_{i+1,j,k} + a_2 u_{i,j+1,k} + a_3 u_{i,j,k+1} \\ & + a_4 u_{i-1,j,k} + a_5 u_{i,j-1,k} + a_6 u_{i,j,k-1} + q_{i,j,k} = 0 \end{aligned}$$

where,

$$\begin{aligned}
a_0 &= \frac{3}{4} (z_{i,j,k} + z_{i-1,j,k} + z_{i,j-1,k} + z_{i,j,k-1} \\
&\quad + z_{i-1,j-1,k} + z_{i,j-1,k-1} + z_{i-1,j,k-1} + z_{i-1,j-1,k-1}) \\
a_1 &= \frac{-1}{4} (z_{i,j,k} + z_{i,j,k-1} + z_{i,j-1,k} + z_{i,j-1,k-1}) \\
a_2 &= \frac{-1}{4} (z_{i-1,j,k} + z_{i,j,k} + z_{i-1,j,k-1} + z_{i,j,k-1}) \\
a_3 &= \frac{-1}{4} (z_{i-1,j,k} + z_{i,j,k} + z_{i-1,j-1,k} + z_{i,j-1,k}) \\
a_4 &= \frac{-1}{4} (z_{i-1,j,k} + z_{i-1,j,k-1} + z_{i-1,j-1,k} + z_{i-1,j-1,k-1}) \\
a_5 &= \frac{-1}{4} (z_{i-1,j-1,k} + z_{i,j-1,k} + z_{i-1,j-1,k-1} + z_{i,j-1,k-1}) \\
a_6 &= \frac{-1}{4} (z_{i-1,j,k-1} + z_{i,j,k-1} + z_{i-1,j-1,k-1} + z_{i,j-1,k-1}) \\
q_{i,j,k} &= \int_{\Omega_{ijk}} h(r) d\Omega, \quad \Omega_{ijk} \text{ is a cubic region around } u_{i,j,k}
\end{aligned}$$

For the 3D problem, we have n^3 equations, one for each grid point on the $n \times n \times n$ mesh. There are $n_u + n_z$ variables, where $n_u = n^3$ and $n_z = (n+1)^3$. Similar to the 2D problem, the Jacobian can be constructed by taking partial derivatives of the discretized equations with respect to each u and z variable. As with the 2D problem, by evaluating the Jacobian for specific values of u and z , we can generate least squares matrices (J^T) with varying aspect ratio.